

Growth mechanism for nanotips in high electric fields

Ville Jansson¹, Ekaterina Baibuz¹, Andreas Kyritsakis¹,
Simon Vigonski^{1,2}, Vahur Zadin², Stefan Parviainen¹, Alvo
Aabloo², and Flyura Djurabekova¹

¹ Helsinki Institute of Physics and Department of Physics, P.O. Box 43
(Pehr Kalms gata 2), FI-00014 University of Helsinki, Finland

² Institute of Technology, University of Tartu, Nooruse 1, 50411 Tartu, Estonia

E-mail: ville.b.c.jansson@gmail.com

Abstract. In this work we show using atomistic simulations that the biased diffusion in high electric field gradients may cause growth of nanotips from small surface asperities. It has long been known that atoms on a metallic surface have biased diffusion if electric fields are applied and that microscopic tips may be sharpened using fields, but the exact mechanisms have not been well understood. Our Kinetic Monte Carlo simulation model uses a recently developed theory for how the migration barriers are affected by the presence of an electric field. All parameters of the model are physically motivated and no fitting parameters are used. The model has been validated by reproducing characteristic faceting patterns of tungsten surfaces that have in previous experiments been observed to only appear in the presence of strong electric fields. The growth effect is found to be enhanced by increasing fields and temperatures.

Keywords: Kinetic Monte Carlo, surface diffusion, electric fields, tungsten, nanotips

1. Introduction

Electric fields may be used as an effective and precise way to manipulate surfaces on the atomic scale [1, 2]. An applied electric field may affect the surface in many ways, such as heating it through resistive Joule heating [3], creating currents that drive the diffusion of vacancies or surface atoms due to an electron wind force [1], evaporation of atoms from the surface [4], or generally roughen the surface by disordering the atomic surface layers [5, 6]. A powerful means of manipulation is to make surface atoms (adatoms) migrate with a biased random walk, where the bias appear when an electric field is applied. How the single surface atom migration becomes biased in electric fields has only recently been explained theoretically [7], but how larger atomic surface structures are affected by fields has not been fully explored. It has been experimentally observed that nanostructures, such as atom islands, surface nanotips or mounds, may appear in electric fields [8–11], but the precise processes and mechanisms have not been studied in detail. It is also known that the application of a high electric in combination with high temperature can be used to sharpen the metal tips used in various applications such as electron microscopy [2, 12, 13].

Of particular interest is the question whether high electric fields may create sharp nanotips. Nanotips are nanofeatures that are of interest because of their optical, mechanical and electrical properties and can be used in many applications, such as electron sources [14, 15], bio-sensors [16–18], plasmonic trapping for the manipulation of nanoscale objects [19], and biocompatible electrodes [20]. Importantly, spontaneous growth of nanotips in high electric fields is also hypothesised to reduce the performance of linear particle accelerators by triggering electric discharges (arcs or breakdowns) in the vacuum of e.g. accelerating structures [21–24]. Nanotips with high enough aspect ratio, sufficiently enhance the field at their apex to cause field emission of electrons and neutrals that in turn may form a vacuum arc plasma [4, 25]. The hypothesis that such nanotips may grow has, however, not yet been proven. The phenomenon is hard to study experimentally as only craters are left after the vacuum arc events and any evidence of possible nanotips can be assumed to be destroyed [26].

The single atom diffusion in electric fields has been studied extensively both experimentally and

theoretically, especially by T T Tsong et al., who showed experimentally in Field-Ion Microscopy (FIM) studies that the adatom migration is biased along the field gradient towards stronger fields [27, 28]. Tsong et al. proposed that the migration energy barrier of a surface atom in a field is dependent of its atomic dipole moment and polarizability [27]. In a recent paper [7], we refined this theory and developed a method for calculating the migration energy barriers in electric fields with Density Functional Theory (DFT). By comparing with DFT calculations of the migration barriers of a W adatom on a W{110} surface, we were able to show that it is not enough to only consider the adatom’s dipole moment and polarizability, but that it is also necessary to take into account the redistribution of the charge density of the whole surrounding system in order to calculate the correct barrier.

Knowing the correct theory for how electric field gradients create a bias in the atom migration processes enables the possibility of implementing this into a Kinetic Monte Carlo (KMC) model which would possibly allow the study of the surface evolution in electric fields on a larger scale. For just the thermal evolution of atomic surfaces, there already exist many KMC models [29–34] and in particular the open-source KMC code Kimocs [35, 36] has been used to study many different nanosystems and -structures, such as nanotips [35], nanowires [37] and nanoclusters [38]. However, there are to date no published KMC models for surface diffusion processes that incorporates the effects of electric fields. Without fields, Cu nanotips have been found in KMC simulations to flatten down due to surface diffusion [35]. In Molecular Dynamics simulations, which are limited to the nanoseconds timescale, both adatom migration [39] and nanotips in fields have been studied [3, 4, 40–42]. For very large nanotips (~ 90 nm) in high fields, a growth process have been observed where the tip is dragged upwards and stretched by the field [4]. However, this process does not explain how a nanotip would be created in the first place. For initiating the formation of a tip, diffusion is a more likely mechanism, as W tip shapening has been observed experimentally [2, 12, 13]. It is worth noting that nanotips have also been observed to grow without any field present, but only in systems with interfaces between two materials: copper and carbon [43], and iron and sapphire [44].

In this work, we will show using KMC simulations that the application of a high electric field on a

tungsten surface may cause diffusion-driven growth of nanotips. For this purpose, we have developed a KMC model where the field effects on the migration energy barriers are based on recent theoretical works. We will also show that our model is able to reproduce and explain previous experimental results where a tungsten tip showed characteristic facet patterning at different electric fields.

The paper is structured as follows: The theoretical basis of the model is summarized in section 2 and its KMC implementation is described in section 3. In section 4, we present the results from the KMC simulations. In section 4.1, we will validate our model by reproducing the particular faceting of a W tip that has been experimentally observed to occur in high electric fields. In section 4.2, we will show that an W hemispherical asperity under an electric field may start to grow and form a nanotip if the fields and temperatures are high enough. In section 4.3 we will show the robustness of the results by studying the sensitivity of the calculated values of the model's central parameters. Finally, we discuss the findings in section 5 and summarize our conclusions in section 6.

2. Theory

The probability rate for a surface atom to make a transition to another position is given by the Arrhenius equation

$$\Gamma = \nu \exp\left(\frac{-E_m}{k_B T}\right), \quad (1)$$

where T is the temperature of the system and k_B is the Boltzmann constant. The attempt frequency ν and the migration energy (or activation energy) E_m will vary depending on the type of transition, but it is common to use the same attempt frequency for any transition, especially if only first-nearest neighbour jumps are used (see e.g. [35, 37, 45–48]). We use the same ν also for second-nearest jumps and exchange processes, as discussed in [49]. The migration energy E_m will depend on the local environment of the transitions; i.e. how many atoms are in the vicinity of the transition and (to a lesser degree) how these neighbour atoms are positioned [48]. For surface atomic processes, it has been found that only considering the number of first- and second-nearest neighbour atoms is enough to characterise the migration energy barriers that are needed to construct KMC simulation models that are precise enough to reproduce Molecular Dynamics (MD) simulations [35] or experimental results [37].

If an external electric field is applied on the surface, this will also affect the migration energy barrier E_m of the surface atom, which will depend on the field strength, the field direction, the field gradient along the atom jump, the type of atom that is jumping

and which elements it is surrounded by. This effect was studied theoretically and described in detail in [7], so we will in the following only summarize the main findings.

Applying an electric field on a metallic surface will rearrange the charge distribution $\rho(\vec{r})$ of the atomic system. In an applied field, the $\rho(\vec{r})$ will also change if the atomic configuration changes, such as in the case of a surface atom making a transition to a neighbour lattice point. This change of $\rho(\vec{r})$ will also change the system dipole moment, $\vec{p} = (p_x, p_y, p_z) = \int \rho \vec{r} dV$, which can be calculated for small atomic systems with DFT, where the system would include an atomic substrate with a free surface, on top of which the jumping adatom is placed [7]. The system needs to be wide enough for the local field enhancement of the adatom not to affect the surface fields at the borders of the system and the substrate needs to be thick enough for the field not to penetrate it. We assume the field to be uniform or having a uniform field gradient at the upper vacuum boarder, above the substrate. For an electric field $F = |\vec{F}|$ in the z direction, perpendicular to the surface, the energy of the system will be given by [7]

$$E(F) = E(0) - \int_0^F p_z(F') dF', \quad (2)$$

where $E(0)$ is the energy without any external field. In [7], it is shown that p_z may for small fields be represented as a Taylor expansion

$$p_z(F) = \mathcal{M} + \mathcal{A}F + O(F^2), \quad (3)$$

where \mathcal{M} is the permanent dipole moment and \mathcal{A} is the polarizability of the system. The energy of the system, equation 2, may now be written as [7]

$$E(F) = E(0) - \mathcal{M}F - \frac{1}{2}\mathcal{A}F^2 + O(F^3). \quad (4)$$

The parameters \mathcal{M} and \mathcal{A} are calculable with DFT and will change when the atomic configuration of the system changes. The migration energy barrier $E_m(F)$ for a surface atom transition jump in an applied electric field F is given by [7]

$$E_m(F) = E_s - E_l = E_m(0) - \mathcal{M}_{sl}F - \frac{1}{2}\mathcal{A}_{sl}F^2, \quad (5)$$

where $E(0)$ is the barrier without any field, $\mathcal{M}_{sl} \equiv \mathcal{M}_s - \mathcal{M}_l$, and $\mathcal{A}_{sl} \equiv \mathcal{A}_s - \mathcal{A}_l$; where the subscript s refer to the system with the transition atom in the saddle point position and the subscript l refer to the same system, but with the transition atom in the (initial) lattice position. If the applied field is not homogeneous, but has a gradient $\gamma \equiv dF/dx$ along the transition direction, which is so small that the difference in the applied field is negligible within a cut-off radius, $R_c \sim 1-2$ lattice constants, i.e. $\gamma R_c \ll F_l$, the migration energy barrier can be written as [7]

$$E_m \approx E_m(0) - \mathcal{M}_{sl}F_l - \frac{\mathcal{A}_{sl}}{2}F_l^2 - \mathcal{M}_{sr}\Delta F - \mathcal{A}_{sr}F_l\Delta F, \quad (6)$$

Table 1. The electronic parameters for equation 6, as calculated for the first-nearest neighbour jump of a W adatom on a W{110} surface with DFT [7].

\mathcal{M}_{sl}	[e m]	$-3.19 \cdot 10^{-12}$
\mathcal{A}_{sl}	[e m ² V ⁻¹]	$3.1 \cdot 10^{-22}$
\mathcal{M}_{sr}	[e m]	$2.735 \cdot 10^{-11}$
\mathcal{A}_{sr}	[e m ² V ⁻¹]	$2.6 \cdot 10^{-21}$

where $\Delta F \equiv F(x_s) - F(x_l) = \gamma(x_s - x_l)$. Here $\mathcal{M}_{\text{sr}} \equiv \mathcal{M}_s - \mathcal{M}_r$ and $\mathcal{A}_{\text{sr}} \equiv \mathcal{A}_s - \mathcal{A}_r$, where the subscript r refer to the system without the transition atom, the reference system. Equations 6 and 5 were confirmed for a W jump on a W{110} surface using DFT calculations in [7]. The \mathcal{M} and \mathcal{A} parameters were calculated for the first nearest neighbour self-diffusion jump on the W{110} and the values are reproduced in table 1.

3. Methods

In this work, we used the open-source KMC code Kimocs [35, 36] together with the field-solver from the code HELMOD [40]. Kimocs was specially developed to study atom diffusion processes on metallic surfaces. It uses a rigid lattice for the atoms, that are either face-centred-cubic (fcc) or body-centred-cubic (bcc). In this paper we use a bcc lattice and a W parameterization, which includes first- and second-nearest jumps. The parameterization also includes a third-nearest neighbour diagonal exchange process, which has been found important for the {100} surface [49, 50]. The implementation in Kimocs treats exchange processes as normal jump processes, but uses the NEB-calculated migration energy barriers of the actual exchange process. Since only atoms of the same element (here W) are used and the atoms thus are indistinguishable, the omission of the actual exchange will not change the evolution nor the dynamics of the system. The parameterization is described in detail in [49]. The attempt frequency $\nu = 4.3 \cdot 10^{14} \text{ s}^{-1}$ was fitted to MD simulations in [49] and is used for all processes.

The probability for any atom transition event is calculated using equation 1. The migration energy barriers in the absence of any electric field $E_m(0)$ are different for all atom transition processes and need to be tabulated prior to the KMC simulations. The individual atom transitions are described by counting the number of first and second nearest neighbours of the initial position (a and b) as well as the final position (c and d). For every process of the same transition distance with the same neighbour configuration (a, b, c, d), the same pre-calculated migration energy $E_m(a, b, c, d)$ is used. We only consider pure metals in our simulations; vacancies are the only possible defects.

Atoms or clusters of atoms are not allowed to be detached from the surface, since these would not be taken correctly into account in the field calculations (see below). Nor do we explicitly account for evaporation, but atoms may become isolated if the surrounding atoms are diffusing away. Such isolated atoms, with no nearest neighbours and one or less second-nearest neighbour atoms, will be removed from the system in order to avoid simulation artefacts. We will however still refer to these removed atoms as “evaporated” for simplicity.

3.1. The field solver

The field is calculated using the field model from the hybrid Molecular Dynamics-electrodynamics code, now known as HELMOD, which is thoroughly described in [40]. In the HELMOD model, the electric field above an arbitrarily rough, but still continuous, metallic surface (see figure 1) is calculated by solving Laplace’s equation

$$\nabla^2 \Phi = 0, \quad (7)$$

where Φ is the electrostatic potential [51]. Using Laplace’s equation instead of the more general Poisson’s equation, which takes into account space charges, is sufficient as we in this model focus on surface processes and do not consider atoms or ions detached from the surface. The field is not allowed to penetrate the surface more than 0.2 nm (about one atomic layer), as has been estimated for metal surfaces [51]. Equation 7 is solved using the finite-difference method on a fine 3D grid with Gauss-Seidel iterations [52]. The field grid is simple-cubic and aligned so that all (rigid) atom positions will coincide with the field grid points. For the cubic bcc unit cell with 2 atoms, there will be $2 \times 2 \times 2$ field grid points in the unit cell, of which 2 coincide with the atomic positions and 6 grid points are free.

At the lower boundary at the metal surface, a Dirichlet type condition, i.e. $\Phi = 0$, is used. At the upper boundary of the vacuum, within which space the field is calculated, a Neumann type condition is used, i.e. $-\nabla \Phi = \pm F \hat{z}$, where F is the external field. For the anode, we define the positive field $F > 0$ to be directed upwards (in the $+\hat{z}$ direction) and in the cathode case, the negative field $F < 0$ is directed downwards, towards the surface (in the $-\hat{z}$ direction).

3.2. Implementation of the field effect into the KMC model

In the KMC simulations, all possible atom transition jumps are assigned a probability rate according to the Arrhenius formula 1, where the migration energy barrier E_m is defined according to the field-dependent

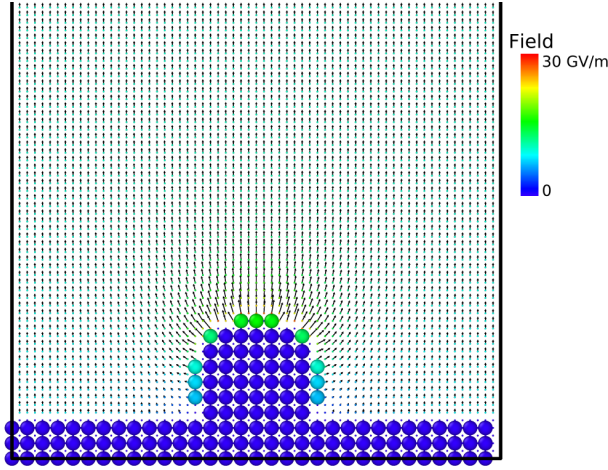


Figure 1. Cross-section of a system with a spherical asperity on a flat atomic surface. Atoms are shown as large spheres, whereas the dots and arrows are grid points in the vacuum, showing the field strengths and directions calculated by the field solver.

formula 6. The field-independent barriers $E_m(0)$ are pre-calculated and tabulated (see [49]).

The surface field magnitude F_l in equation 6, which is the field assumed to be interacting with a surface atom at a lattice point position, is in Kimocs defined as the field value calculated by the field solver at a distance $h = 1$ nm along the field lines, roughly perpendicularly, above the surface atom (figure 2). This way the field value is only minimally affected by the local field enhancement of the atom itself, in accordance with the theoretical definition of F_l , as described in section 2. The direction of the field vector at the surface atom will be calculated by taking the average of the non-zero field vectors of the 26 surrounding field lattice points, as the field is not calculated by the field-solver for the points coinciding with atoms. The field lattice points are in a simple-cubic field lattice and will have a spacing that depends on the atomic lattice; for a bcc lattice with a $\langle 100 \rangle$ z orientation, as in this work, the field lattice will have a lattice parameter $a_0/2$, where a_0 is the lattice parameter of the atomic bcc lattice. This way, all surface atoms will be assigned a field value F_l , which will be positive for an anode field and negative for a cathode field.

Surface vacancies, i.e. an empty atomic lattice positions with at least one first-nearest neighbour atom, will be assigned field values F_v the same way, except that the direction of the field vector is taken directly from the field solver at the field grid points coinciding with the vacancies; i.e. no average is needed as for the atoms. The magnitude of the fields are still taken at the distance h above the surface vacancies.

For every surface atom, the field gradient γ needs to be calculated in the direction of every possible atom

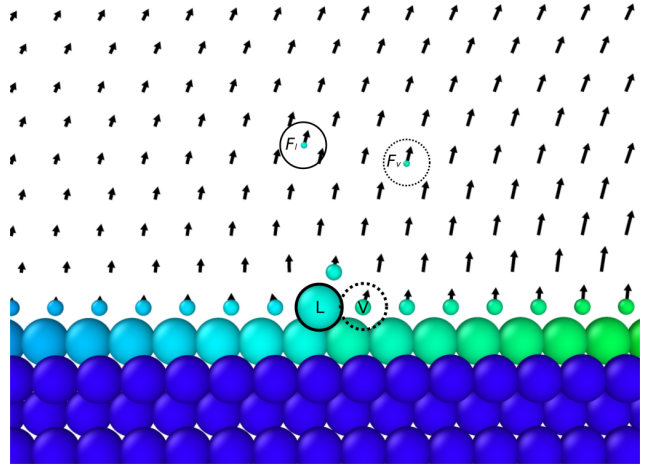


Figure 2. Cross-section of a surface under a field gradient. Atoms are depicted as large spheres and surface vacancies as small spheres. Shown are also the field vectors, calculated by the field solver for the of the simple-cubic field lattice points. The surface atom L , marked by a circle, at a lattice position, will be assigned the field magnitude F_l of a field point at a distance $h = 1$ nm above the surface, marked by a thin circle. Similarly, the surface vacancy V , marked with a dotted circle, is assigned the field magnitude F_v from the position marked with a thin dotted circle, 1 nm (h) along the field lines above the vacancy. The gradient for atom L to jump to V is given by $(F_v - F_l)/d$, where d is the distance between the field points of F_v and F_l . The colours of the atoms and vacancies corresponds to the assigned field magnitudes, with dark blue for the zero fields of the bulk atoms.

jump. In Kimocs, this is done as

$$\gamma = \frac{F_v - F_l}{d_f}, \quad (8)$$

where F_l is the field of the jumping atom, F_v is the field of the vacancy at the target lattice position, and d_f is the distance between the two field lattice points at a distance h above the surface where the magnitudes of F_l and F_s were actually calculated by the field solver (figure 2).

The difference in field between the saddle point and the initial lattice point $\Delta F \equiv F_s - F_l$, as defined in equation 6, is calculated as

$$\Delta F = \gamma d, \quad (9)$$

where d is the distance between the saddle point and the initial position of the jumping atom. In this work, we always assume the saddle point to be exactly half-way of any atom jump or exchange process. The ΔF values have to be recalculated for every possible atom jump in the system every time the field has been recalculated by the field-solver, which happens after every KMC step. Calculating the field is the most costly part of the simulation and uses ~ 99 % of the CPU time.

To estimate the errors of F_l and γ (and by extension ΔF), consider the simple system with an

adatom on a perfectly flat surface under a field gradient, shown in figure 2. Removing the adatom at L and comparing the field strengths at positions L and V with the F_l and F_v values, respectively, gives a difference of 3.4 %. Comparing the values at the points of F_l and F_v with and without the adatom (L) present, gives a difference of less than 1 %. Comparing the gradients γ with and without the adatom (L) present, gives a difference of 13 %. Since removing atoms individually in order to precisely calculate the field without their own field-enhancement would require too many calls to the computationally expensive field solver, these errors can be considered quite acceptable in comparison.

The \mathcal{M} and \mathcal{A} parameters in equation 6 were calculated for a first-nearest jump of a W atom on a W{110} in [7] and are reproduced in table 1. In this work these values are used for any atom jump or exchange process, as a first approximation, which is still good enough to enable the reproduction of experimental results, as will be shown in section 4.1.

4. Results

4.1. Comparison with experiments: faceting in fields

S Fujita and H Shimoyama [53] have reported an experiment where a W tip with a rounded apex of a curvature ~ 206 nm was subjected to several 30 s periods of increasingly higher anode fields in an ultra high vacuum. The tip was kept at a temperature of 2300 K. The shape of the tip was observed after every cycle with a Scanning Electron Microscope (SEM) and by applying a smaller cathode field in order to observe its field emission pattern. They observed a characteristic faceting pattern on the W tip that depended on the strength of the local anode fields (which they denote F_r in [53]). The different observed stages of the faceting were as follows [53]:

- (i) The original W tip is orientated in the $\langle 100 \rangle$ direction, relative to the field. It is rounded by a flashing procedure.
- (ii) A field of 2.5 GV/m was applied and the {110}, {211}, and {100} facets were seen to begin growing in size.
- (iii) The field was further increased to 3.51 GV/m. The {110}, {211}, and {100} facets were seen to grow even more in size and the emitter obtained a polyhedral shape.
- (iv) With a field of 3.56 GV/m, the {211} facets suddenly start to shrink and the {110} facet starts to grow.
- (v) At 4.00 GV/m, the {211} facets have completely disappeared and the {110} facets dominate.

- (vi) At 4.20 GV/m, a large square-formed top {100} facet is formed with four corners. The field-emission pattern shows four bright spots at the positions of the four corners, where four microprotrusions could be observed with SEM.
- (vii) Increasing the field even further, to 4.49 GV/m, creates an “overremolding” state where the surface becomes irregular and the emission pattern is not any more predictable.

In order to reproduce with Kimocs these above listed experimentally observed stages of the W tip evolution from [53], we simulated a 3 nm high W hemisphere with a 10 nm radius (figure 3(a)) on a substrate with a perfectly flat W{100} surface. The flat substrate is only needed to create a lower boundary for the system and the field solver; for the comparison with the experiment, we are only interested in the evolution of the curved surface of the hemispherical tip.

The system was a cubic box with every side of length $64a_0$, with the W lattice parameter $a_0 = 3.14339 \cdot 10^{-10}$ m. The substrate was $3a_0$ (0.94 nm) thick, leaving 16 nm of vacuum above the apex of the 3 nm hemispherical tip on the substrate. This is more than enough vacuum to make the field homogeneous at the upper boundary of the system. The thickness of the substrate is not important, since almost all atomic movement will happen on the tip due to the locally enhanced field, whereas the strongly bonded atoms on the perfectly flat surface of the substrate will not move significantly. Periodic boundaries were applied in the lateral x and y directions. The bottom atom layer of the substrate was fixed.

Different electric fields were applied in the system by solving the Laplace equation in the vacuum part of the system, above the surface, as described in section 3.1. Thirteen different applied anode fields between 2.5 and 60.0 GV/m were used, defined as the surface field at the centre of the top {100} facet of the initial hemisphere and should be comparable to the applied fields in the experiment of Fujita and Shimoyama. The corresponding fields at the upper boundary of our vacuum system were in fact between 1.48 and 35.4 GV/m, respectively. The simulations were stopped after 20 ns simulated time had passed, which corresponds to between $7.4 \cdot 10^5$ and $8.7 \cdot 10^5$ KMC steps, or about four weeks in CPU time.

The final surfaces after the simulations with the different applied fields are, for selected cases, shown in figure 3 (top views) and figure 4 (perspective views). The initial system is shown in figures 3(a) and 4(a). As mentioned before, the hemispherical tip has a curvature that, for computational reasons, is ~ 20 times smaller than the curvature of the tip in Fujita’s experiment. Because the tip is smaller, already the initial tip displays small facets: the top {100}, the four

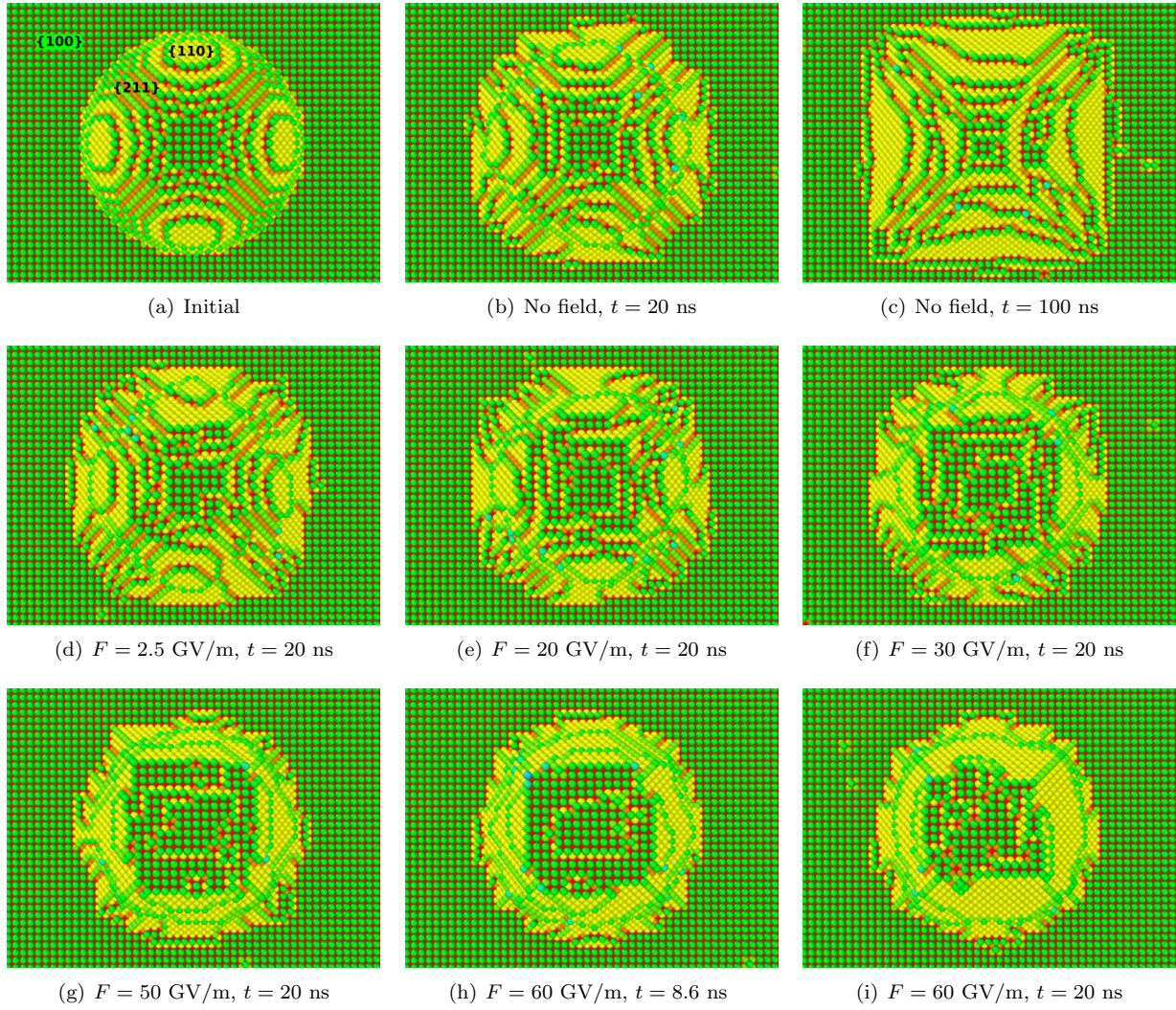


Figure 3. Top view of the simulations of the hemispherical tip system (a) at different applied fields. (b)–(c) shows the same simulation of the hemisphere after 20 ns and 100 ns, respectively, without any field. In (d)–(g), the system is shown after 20.0 ns with different applied fields. (h) and (i) show the same simulation at an applied field of 60 GV/m after 8.6 ns and 20 ns, respectively. The atoms are coloured according to the coordination numbers to emphasise the different facets.

$\{110\}$, and the four $\{211\}$ facets. These will be the same facets as observed in the early faceting of the tip in Fujita’s experiment (ii) because of the identical lattice orientation $\langle 100 \rangle$.

Figures 3(b)–3(c) and 4(b)–4(b) show the tip after 20 ns or 100 ns without any field for reference. In the no-field case, it can be seen that the small initial top $\{100\}$ facet has actually decreased in size and the $\{211\}$ facets have grown.

In figure 3(d), a field of 2.5 GV/m has been applied and the top $\{100\}$ facet is now more prominent than in the case without field [figure 3(b)–3(c)]. The $\{211\}$ facets are larger than in the initial case [figure 3(a)], but not much different to the no-field case. Figure 3(d) seems to roughly correspond to Fujita’s stages (ii) or (iii).

With an applied field of 20 GV/m, shown in figure 3(e), the $\{211\}$ facets start to decrease and the $\{110\}$ facets start to grow, corresponding to Fujita’s stage (iv).

With an applied field of 30 GV/m [figure 3(f)], the $\{211\}$ facets have completely disappeared and the $\{110\}$ facets dominates, as also happened in Fujita’s stage (v).

With an applied field of 50 GV/m, a clear, fairly quadratic, top $\{100\}$ facet is formed, as can be seen in figures 3(g) and 4(d). This facet is formed as atoms along the side $\{110\}$ have a biased diffusion towards the higher fields at the edge of the $\{100\}$ facet. However, for an edge atom to overcome the edge onto the $\{100\}$ facet, a barrier between 0.8 and 3.6 eV needs to be overcome, which is relatively high compare to the

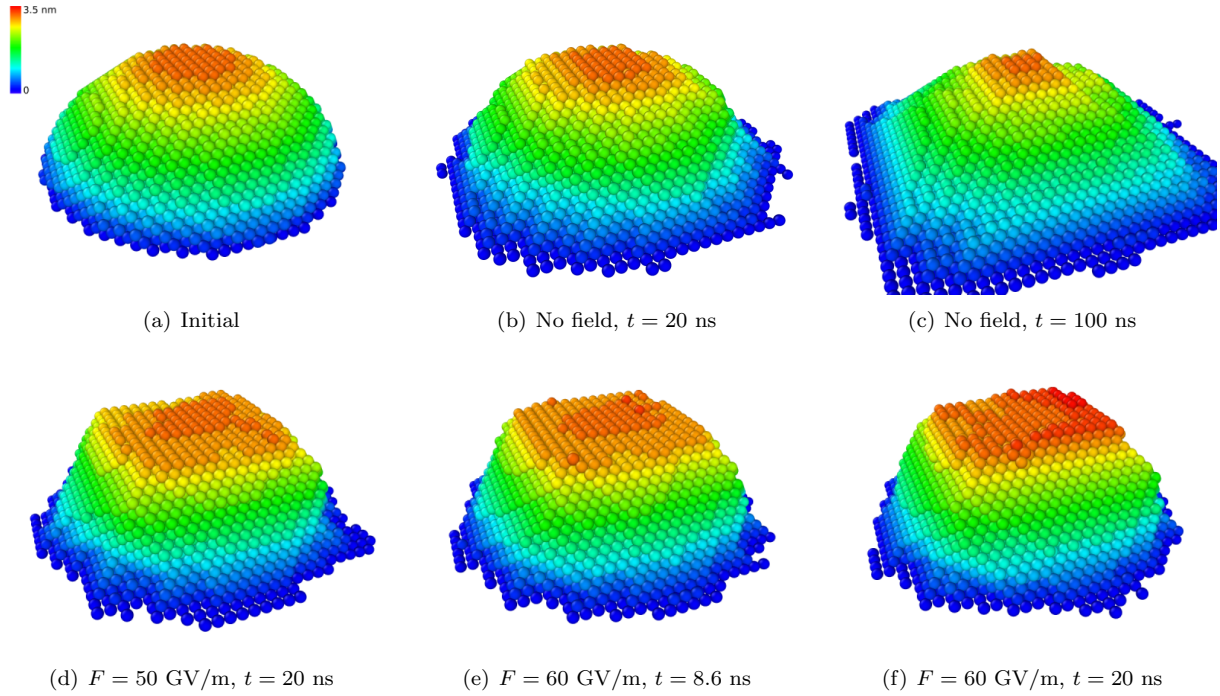


Figure 4. Perspective views of the hemispherical tip: (a) initial, (b)–(c) the same simulations after 20 ns and 100 ns, respectively, without field; (d) with a 50 GV/m applied field after 20 ns; (e) and (f) show the same tip with a 60 GV/m applied field after 8.6 ns and 20 ns, respectively. The atoms are coloured according to the height from the substrate (not shown). The figures are made with Ovito [54].

0.6 eV barrier of the simple jump on the side $\{110\}$ facets. The end result is that the $\{110\}$ islands migrate towards the $\{100\}$ edge in the same time as they grow in size. The tip itself will not grow in height (at this stage), but the $\{110\}$ facets will grow sideways until they fill up the corners of the tip, where initially were $\{211\}$ facets, and in the same time growing the corners of the top $\{100\}$ facet. This is in contrast to the case with no field [figures 3(b)–3(c)], where the $\{211\}$ and $\{110\}$ facets grows and connects with the substrate, where new layers slowly form, making the tip wider. The top $\{100\}$ facet, on the other hand, almost completely disappear.

An slightly more pronounced $\{100\}$ facet is also formed with an applied field of 60 GV/m after 8.6 ns, as shown in figures 3(h) and 4(e). This is in good agreement with the large $\{100\}$ top facet Fujita and Shimoyama observed in their stage (vi), even though we have used higher fields than they reported. The obtained shape of the tip with the large $\{100\}$ facet is clearly different than the tip shape obtained in the case with no field, figures 3(b)–3(c), indicating that the obtained evolution is truly an effect of the applied electric field.

Continuing the simulation with the applied field of 60 GV/m until 20 ns, new higher structures are starting to build up on top of the $\{100\}$ facet, as shown

in figures 3(i) and 4(f). This evolution is reminiscent of Fujita’s “overremoulding” stage (vii).

4.2. Nanotip growth on W surfaces

In the previous section we saw that the KMC model is able to reproduce the surface evolutions in electric fields observed in experiments. In this section we investigate whether fields may cause the formation of nanotips: what kind of field strengths are needed to promote growth, the influence of the temperature, and whether there is a difference between the influence of anode and cathode fields.

In these simulations, we used as starting point a smaller hemispherical asperity with a height of 2.0 nm and a radius of 2.8 nm, placed on a W $\{100\}$ surface [figure 5(a)]. The system was $32a_0$ wide in the lateral x and y directions and $64a_0$ in the z direction. The substrate was $3a_0$ thick with the lowest atom layer fixed. Periodic boundary conditions were applied in the x and y directions. Different initial local fields between 0.4 and 72 GV/m, measured on the top facet of the initial asperity, were used. These fields corresponds to applied external fields between 0.3 and 50 GV/m, measured at the upper boundary of the vacuum system. The locally enhanced fields, measured at a distance $h = 1$ nm above the initial tip, were between 0.4 and 73 GV/m. Two different temperatures, 2000 K

and 3000 K, were used. Both are well below the melting temperature of W. Corresponding negative applied field values were used for the cathode case, but only one temperature, 3000 K, was used. The simulations were stopped after $1.5 \cdot 10^6$ steps or before that if a maximum height of 6.4 nm was reached. This corresponds to simulated times between 6.9 and 36 ns at 3000 K and 0.1 to 1.5 μ s at 2000 K. Generally, longer time scales are reached with lower fields for the same number of steps, since higher fields generally lower the migration barriers and thus shorter the average time steps. The case with strongest growth, with an initial local anode field $F = 72$ GV/m at 3000 K, is shown in figure 5. The same simulation is also shown in figure 6 where the atoms are coloured according to their original z coordinates, in order to show how individual atoms have diffused. It can be seen that even atoms from the substrate (blue) have been able to diffuse almost to the apex of the nanotip. The maximum nanotip height for the different initial local fields and temperatures are shown in figure 7.

The growth is observed to be enhanced by higher temperatures and higher field strengths. Some growth is observed at 3000 K for all applied anode fields, but the growth is more significant above 30 GV/m. The maximum growth, to a height of 6.3 nm, is found with the highest temperature and field, i.e. at 3000 K with an initial local field of 72 GV/m. This gives a height increase of a factor 3.1. With cathode fields, at 3000 K, the initial hemispherical nanotip flattened at all field strengths and no growth was observed.

4.3. Sensitivity of the model parameters

To check the sensitivity of the four electronic \mathcal{M} and \mathcal{A} parameters, the best case of the same system as in section 4.2, with 3000 K and an initial local field of 72 GV/m, was rerun with the electronic parameters varied separately by ± 10 % or ± 20 % to see how the nanotip growth is affected.

In figure 8(a) is shown the maximum nanotip height (out of 10 statistical runs) for different variations of the electronic parameters. The reference case (0 %) is done with 50 statistical runs. It can be seen that even if one of the parameters are changed by 20 %, the nanotip will still grow significantly at this field and temperature. The most sensitive parameter is A_{sr} which, when reduced by 20 %, only grows by a factor ~ 2.2 to 4.3 nm, which is still a significant growth. If any of the other parameters are varied, a height between 5.5 and 6.2 nm is reached, which is not significantly different from the height of the reference, (5.8 ± 0.5) nm. If any of the parameters are individually varied by only ± 10 %, the reached average maximum heights are all within the even smaller span of 5.0 and 6.1 nm.

To better get the effect of the individual \mathcal{M} and \mathcal{A} parameters, the average growth velocity of the tip, defined as the difference in nanotip height divided by the time it took to reach the maximum height, is shown in figure 8(b). It can be seen that increasing \mathcal{M}_{sl} decreases the growth velocity, which is the opposite trend as given by varying \mathcal{A}_{sl} or \mathcal{A}_{sr} . Varying \mathcal{M}_{sl} gives no clear trend in either direction.

We also checked the sensitivity of the h parameter, which gives the distance above the surface where the surface fields F_l and F_v are calculated by the field solver for every atom and surface vacancy. The same system as in section 4.2 was again simulated at 3000 K at external fields between 8.0 and 50 GV/m, but with h varied between 0.5 and 1.2 nm. Changing h will change the values of the fields F_l , F_v and the gradients γ . The local fields will subsequently also be different for the same external fields, as measured at the upper boundary of the vacuum.

As is shown in figure 9, with smaller h values, the growth is enhanced and more significant at smaller external fields. With $h = 0.5$ nm, significant growth appears already at external fields between 1 and 20 GV/m, which corresponds with this h to the initial local fields between 18 and 37 GV/m. With $h = 0.5$ nm and an external field of 50 GV/m, too many atoms started to evaporate (see section 3) for the results to be reliable.

5. Discussion

The KMC code Kimocs and its (a, b, c, d) parameterization model for the atom transitions were originally developed for studying only thermally activated diffusion processes on surfaces and has been successfully used in several such studies [35, 37, 38, 48], where the simulation results have shown good agreement with both MD simulations and experimental results. The W parameterization in this work includes not only first-nearest neighbour atom jumps, but also second-nearest neighbour jumps. The second-nearest jumps are particularly important on the $\{100\}$ surface, as no first-nearest neighbour jumps are possible there. Additionally, the parameterization includes a third-nearest neighbour exchange process, as its barrier 1.95 eV is comparable to the other jumps and therefore may be of significance. The W parameterization has already been discussed in detail and validated in a previous paper [49].

5.1. The field model

In order to extend the KMC model to include electric field, we have used the recently developed theory for how an applied field affects the atom migration barriers [7], summarized in section 2. The electric field is solved

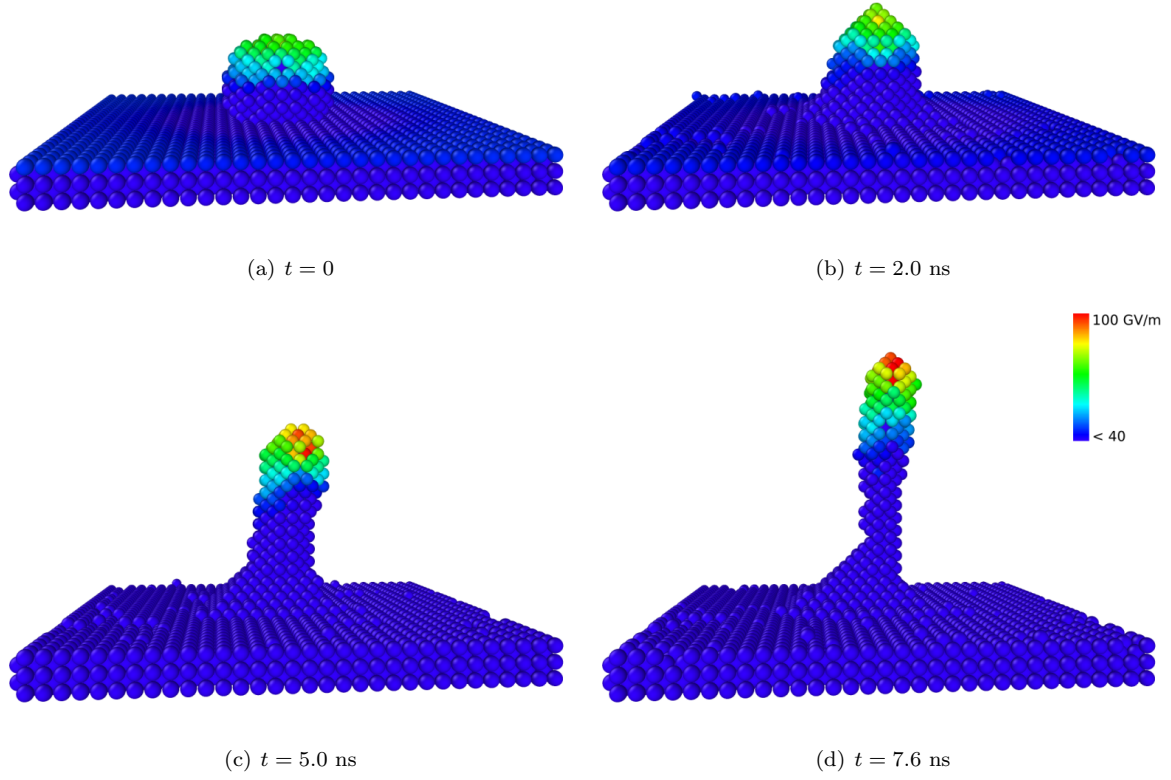


Figure 5. Time frames showing the growth process of a W nanotip at different stages in an applied electric field of 50 GV/m (initial local field 72 GV/m) at 3000 K, starting from a hemispherical asperity (a). The initial asperity (a) is 2.0 nm high and the final nanotip (d) is 6.3 nm high. The atoms are coloured according to the local surface field strength. For an animation, see the Supplementary Materials.

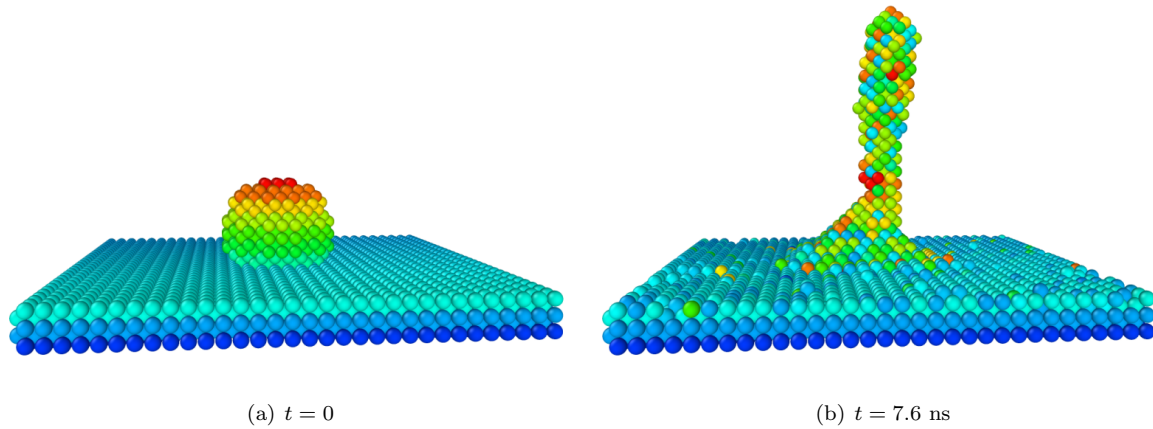


Figure 6. The same nanotip growth simulation as in figure 5, but with the atoms coloured according to their initial position (a) in order to show how the individual atoms have diffused.

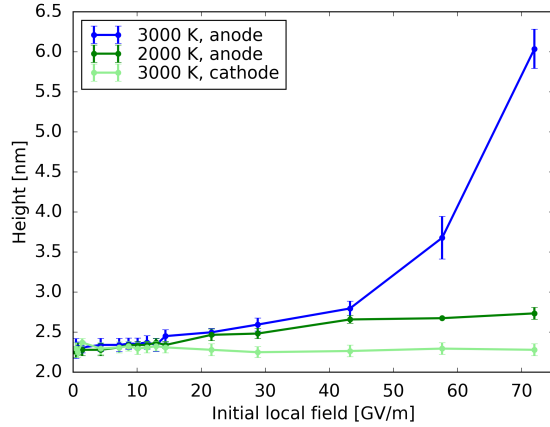


Figure 7. Maximum height reached during a $1.5 \cdot 10^5$ steps simulation (out of ten parallel runs) for different temperatures and initial fields. The initial nanotip height was 2.0 nm.

in the vacuum space above the atomic surface using the established field solver from HELMOD [40], which has been previously used in several Molecular Dynamics studies where a field was present, e.g. [3, 41]. The effect of the electric field on the migration energy barriers is given by equation 6, described in section 2. The full theoretical derivation of equation 6 is given in [7].

Some approximations were unavoidable in the model. In order to obtain the precise field-dependent migration energy barrier $E_m(F)$ for every possible surface atom jump, the parameters \mathcal{M}_{sl} , \mathcal{A}_{sl} , \mathcal{M}_{sr} , and \mathcal{A}_{sr} (henceforth simply the \mathcal{M} and \mathcal{A} parameters) would ideally need to be calculated with DFT for every such process (there is no field present in bulk processes). Since 5–10 separate DFT calculations are needed to obtain the \mathcal{M} and \mathcal{A} parameters for a single atom transition process and there are 100–1000 possible surface atom transition processes, a number of $500\text{--}10^4$ DFT calculations would be needed to obtain a complete set of the \mathcal{M} and \mathcal{A} parameters. This is beyond the scope of this work. Instead we make the assumption that the \mathcal{M} and \mathcal{A} values obtained for the single process of a W atom jump on a W{110} surface in [7] (table 1) are approximately correct for any W atom transition on a W surface. This assumption is supported by the good agreement between our KMC simulations and the experimental observation of the tungsten surface evolution in fields, as presented in section 4.1, but also by the low sensitivity that the nanotip growth simulations showed with regards to the \mathcal{M} and \mathcal{A} parameters in section 4.3. These results will be further discussed in the following sections 5.2 and 5.3.

Another uncertainty in the model is how to define and calculate the fields associated with the lattice points F_l , the difference in field between the saddle

point (F_s), and the lattice point, $\Delta F = F_s - F_l$, (as used in equation 6). As was already described in section 3.2, F_l , F_s , and ΔF depend on the parameter h , which is the distance above the surface, along the field lines, that the field for a particular surface atom or surface vacancy is calculated by the field-solver. The distance h needs to be large enough for the field not to be affected by the local field enhancement of the adatom itself, as this enhancement is already included in the \mathcal{A} and \mathcal{M} parameters [7]. If, on the other hand, h would be too large, F_l and F_v would both approach the nominal external field of the system, i.e. the limit at the upper boundary of the vacuum, and the gradient γ and ΔF would approach zero. In section 3.2 we showed for a flat surface with a field gradient that with our chosen value $h = 1$ nm, the error for the fields F_l and F_v are 3.4 % and for the gradient 13 %. In section 4.3, we showed that nanotip growth happens even if h is varied by ± 20 %, with the growth enhanced with smaller h .

The described choices for how F_l and ΔF are calculated have the advantage of being easily applicable to any arbitrarily rough surface. The easy applicability is important since F_l and ΔF have to be recalculated for every atom and every possible atom jump in the system, respectively, after every time the field-solver has been called, i.e. at every KMC step.

5.2. Faceting in fields

In section 4.1, we showed that our KMC model is able to qualitatively reproduce the different main characteristic faceting patterns of the surface evolution of a W tip in different electric fields, as observed in experiments by S Fujita and H Shimoyama [53]. Certain differences between the simulations and the experiment should be pointed out. In the experiment, a single tip was observed under fields that were increased in a stepwise manner, with exposure durations of ~ 30 s at each step, between the observations. This kind of time scales are hard to reach with KMC methods, where already reaching μ s time scales takes weeks of CPU time with the current model. In order to speed up the simulations, we also use a much smaller curvature (10 nm) of the W tip, compared to the experimental tip ($\sim 2.06 \cdot 10^{-7}$ m).

Fujita and Shimoyama's interpretation [53] of their experiment is that the energetically favourable surface changes depending on the strength of the applied field, which is also our interpretation. Therefore, the order of the stages with the different fields does not matter as the surface will, independently of the initial shape and given enough time, relax to the energetically favourable shape that depends on the currently applied field strength. Our simulations with fields indeed show the initially perfectly hemispherical tip will transform to very similar faceting patterns that vary with the

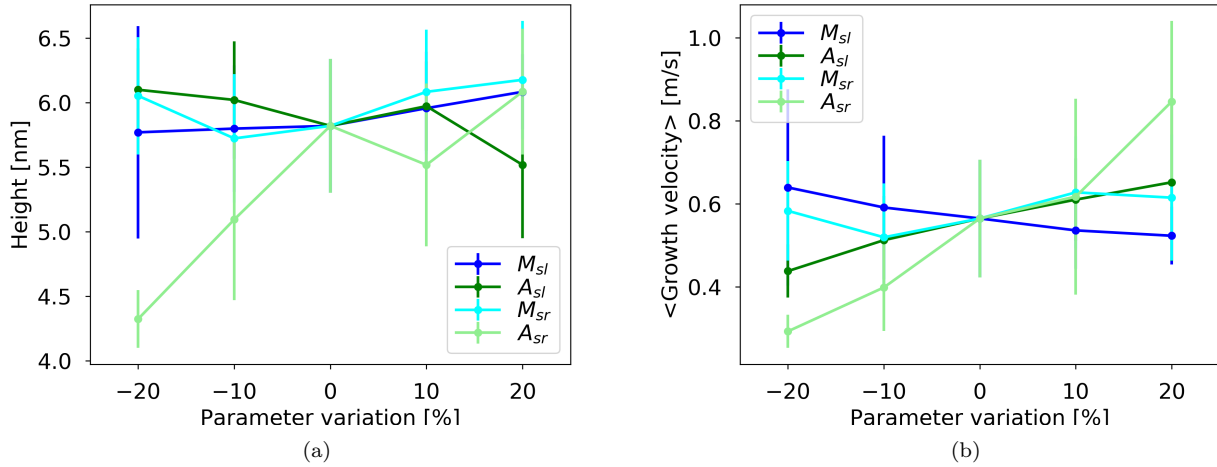


Figure 8. Sensitivity of the electronic \mathcal{M} and \mathcal{A} parameters. The best case from section 4.2 is simulated with each of the four \mathcal{M} and \mathcal{A} parameters separately varied by $\pm 10\%$ or $\pm 20\%$. The reference case is included as 0 %. Figure (a) shows the nanotip average maximum heights over ten runs, (b) shows the average growth velocity to reach the maximum height. Error bars correspond to the standard deviation.

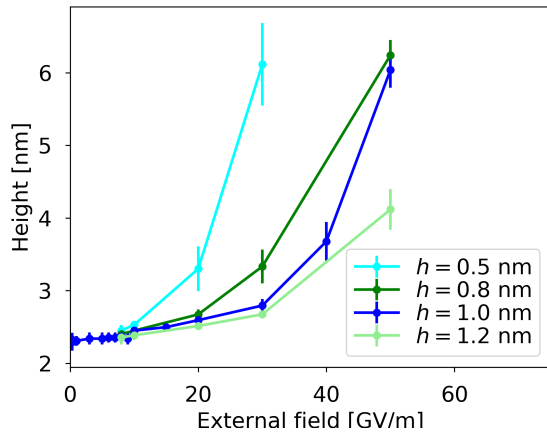


Figure 9. Sensitivity of h , the distance above the surface where the surface fields F_l and F_v are calculated by the field solver. The maximum nanotip height is shown for different external fields (measured at the upper vacuum boundary of the simulation box). As standard $h = 1.0$ nm is used. Every data point is the average of ten runs.

strength of the applied field in a corresponding way as seen in the different stages in the experiment, although our model seems to require much higher fields.

Fujita and Shimoyama observe the large top $\{100\}$ facet to form at an estimated average field of 4.20 GV/m, whereas, in the simulations, a similar facet is observed [figures 3(g) and 3(h)] to form at a higher field of 50.0 GV/m; a difference of a factor ~ 12 . This difference is overestimated by the fact that in Ref. [53] the local electric field was estimated using the same initial voltage conversion factor (denoted kr in [53])

for the entire remolding process. This is not accurate, since from Fujita's Fig. 4a, the extraction voltage for the same field emitted current drops by a factor of about 2.5 during the remolding process due to the tip sharpening. This implies that the conversion length kr , i.e. the ratio between voltage and local field is also reduced (the field enhancement increased) by a similar factor. Therefore a more accurate estimation would be that the local field at the tip is about 11 GV/m in that phase of the experiment, which reduces the discrepancy to a factor of ~ 4.5 . This exaggeration of the field, necessary to reproduce the tip behaviour in the simulations, is needed in order to accelerate the processes, since the time scales of seconds that are available in the experiment are not accessible by our atomistic simulations.

Finally, note that the KMC simulations of the W clusters in [49] also showed large $\{100\}$ facets, indicating that these may be relatively stable, but in simulations of the hemispherical tip (with the same curvature), the $\{100\}$ facets completely disappeared if a field was not present. The reproduction of the large top $\{100\}$ facet is of particular importance, as it is only seen to form when a strong enough electric field is present, in both the experiment of Fujita and Shimoyama [53] and in our simulations. This, together with the observations of the other faceting stages is a strong validation of the simulation model.

5.3. Nanotip growth

In section 4.2, we demonstrated that the migration bias given by surface field gradients may create a nanotip growth mechanism, given that the applied fields and

the temperatures are high enough. Our simulations show that a 2 nm high hemispherical W tip with a 2.8 nm curvature at 3000 K starts to show significant growth at an initial anode field of 9 GV/m at the tip apex, whereas at 2000 K, the growth speed is significantly reduced and only some minimal growth can be seen within the simulated time frame of ~ 1 μ s. For cathode fields, we do not see any clear growth with the current model. The dependence of the sign of the field (anode or cathode) comes from the \mathcal{M} and \mathcal{A} parameters in equation 6, which are dependent on the electrical properties on the material; in this case tungsten (see also the discussion in section 5.1).

The simulations of the small tip in section 4.2 and the larger curved surface in section 1 show that the growth processes will be initiated where the field gradients are strongest, such as at the tip apexes or at edges. Elsewhere, such as on the flat substrate or at the base of the tips, where the fields are also weaker, only minimal changes of the surface can be seen. Thus, in order to initiate growth of a nanotip, a nucleation point in form of some kind of asperity with a high enough gradient is needed.

In this work, we are studying the diffusion growth mechanism, but it is worth noting that we do not take into account thermal and ionic evaporation processes that would give the opposite effect. These kind of processes may play a significant role at fields 30–50 GV/m and above. Atoms at the tip apex may be evaporated if the local fields are strong enough and thereby reduce the tip growth. However, a precise description of the competing thermal and field-assisted atom evaporation processes is beyond the scope of this work.

We also note that this work only considers nanotips on the bcc{100} surface, as the field solver currently only can handle this particular surface. In [35] different stabilities of nanotips of different lattice orientations were found. Tips on other surfaces than {100} may therefore behave and grow differently than observed here. Our results are neither necessarily general for other materials than tungsten, since the \mathcal{M} and \mathcal{A} parameters are material-dependent.

In general, our results make it highly plausible that nanotips may form on metallic surfaces if a high electric field gradient and some kind of nucleation point are present. Such nanotip growth may be one explanation for the formation of vacuum arcs (or breakdowns) in high electric fields, such as in accelerating structures [21–24]. The nucleation points, small asperities on the surface, may possibly be caused by dislocation movement close to the surface and dislocation activity in surfaces under high fields has been correlated to breakdowns in a recent statistical model [23]. Very large nanotips (~ 90 nm high) may, on

the other hand, emit enough electrons and neutrals to initiate a vacuum arc plasma [4]. Our work provides a plausible mechanism for how these large nanotip may form, where small protrusions caused by dislocations acting as nucleation points for the biased surface atom diffusion in the high fields, that build up nanotips until they are large enough to start field emission.

6. Conclusions

In this work, we have identified a growth mechanism for nanotips on metal surfaces in high electric fields. This was done using a general-purpose Kinetic Monte Carlo model for simulations of diffusion processes on arbitrarily rough tungsten (W) surfaces in high electric fields. We have validated the model by reproducing the experimentally observed characteristic faceting of a large hemispherical tungsten surface in high electric fields and in particular the formation of a large {100} facet, which would not happen without a field present.

The fields and temperatures at which small W surface asperities may grow into nanotips were investigated and we have found that growth due to diffusion on W surfaces is more significant with higher local fields and higher temperatures. The model clearly shows the plausibility of the formation of nanotips in high electric fields by atom diffusion. The results support the hypothesis that vacuum arcs in high-field environments may be caused by such spontaneous formations of nanotips.

Acknowledgments

V Jansson was supported by Academy of Finland (Grant No. 285382) and Waldemar von Frenckells Stiftelse. A Kyritsakis were supported by a CERN K-contract (No. 47207461). E Baibuz was supported by the CERN K-contract (No. 47207461) and the doctoral school DONASCI of University of Helsinki. The work of V Zadin and A Aabloo was supported by Estonian Research Council Grants PUT1372 and IUT20-24. F Djurabekova acknowledges gratefully the financial support of Academy of Finland (Grant No. 269696). Computing resources were provided by the Finnish IT Center for Science (CSC) (persistent identifier urn:nbn:fi:research-infras-2016072533).

ORCID iDs

V Jansson <https://orcid.org/0000-0001-6560-9982>
 E Baibuz <https://orcid.org/0000-0002-9099-1455>
 A Kyritsakis <https://orcid.org/0000-0002-4334-5450>
 S Vigonski <https://orcid.org/0000-0002-2849-2882>
 V Zadin <https://orcid.org/0000-0003-0590-2583>
 S Parviainen <https://orcid.org/0000-0003-4571-4640>

A Aabloo <https://orcid.org/0000-0002-0183-1282>
 F Djurabekova <https://orcid.org/0000-0002-5828-200X>

References

- [1] Strosio J A and Eigler D 1991 *Science* **254** 1319–1326
- [2] Tsong T T 2005 *Physica A: Statistical Mechanics and its Applications* **357** 250–281
- [3] Parviainen S, Djurabekova F, Timko H and Nordlund K 2011 *Computational Materials Science* **50** 2075–2079
- [4] Kyritsakis A, Veske M, Eimre K, Zadin V and Djurabekova F 2018 *Journal of Physics D: Applied Physics* **51** 225203
- [5] de Knoop L, Kuisma M J, Löfgren J, Lodewijks K, Thuvander M, Erhart P, Dmitriev A and Olsson E 2018 *Physical Review Materials* **2** 085006
- [6] de Knoop L, Kuisma M J, Löfgren J, Lodewijks K, Thuvander M, Erhart P, Dmitriev A and Olsson E 2019 *Microscopy and Microanalysis* **25** 1830–1831
- [7] Kyritsakis A, Baibuz E, Jansson V and Djurabekova F 2019 *Phys. Rev. B* **99**(20) 205418 (Preprint <https://arxiv.org/abs/1808.07782>) URL <https://arxiv.org/abs/1808.07782>
- [8] Whitman L, Strosio J A, Dragoset R A and Celotta R 1991 *Science* **251** 1206–1210
- [9] Mendez J, Gómez-Herrero J, Pascual J, Saenz J, Soler J and Baro A 1996 *Journal of Vacuum Science & Technology B: Microelectronics and Nanometer Structures Processing, Measurement, and Phenomena* **14** 1145–1148
- [10] Mayer T, Houston J, Franklin G, Erchak A and Michalske T 1999 *Journal of applied physics* **85** 8170–8177
- [11] Dulot F, Eugene J, Kierren B and Malterre D 2000 *Applied surface science* **162** 86–93
- [12] Bettler P C and Charbonnier F M 1960 *Phys. Rev.* **119**(1) 85–93 URL <https://link.aps.org/doi/10.1103/PhysRev.119.85>
- [13] Dyke W P, Charbonnier F M, Strayer R W, Floyd R L, Barbour J P and Trolan J K 1960 *Journal of Applied Physics* **31** 790–805
- [14] Zhou J, Gong L, Deng S Z, Chen J, She J C, Xu N S, Yang R and Wang Z L 2005 *Applied Physics Letters* **87** 223108
- [15] Bormann R, Strauch S, Schäfer S and Ropers C 2015 *Journal of Applied Physics* **118** 173105
- [16] Cherevko S and Chung C H 2009 *Sensors and Actuators B: Chemical* **142** 216–223
- [17] Kabashin A, Evans P, Pastkovsky S, Hendren W, Wurtz G, Atkinson R, Pollard R, Podolskiy V and Zayats A 2009 *Nature materials* **8** 867
- [18] Caldwell J D, Glembocki O, Bezares F J, Bassim N D, Rendell R W, Feygelson M, Ukaegbu M, Kasica R, Shirey L and Hosten C 2011 *ACS nano* **5** 4046–4055
- [19] Wang K and Crozier K B 2012 *ChemPhysChem* **13** 2639–2648
- [20] Brüggemann D, Wolfrum B, Maybeck V, Mourzina Y, Jansen M and Offenhäusser A 2011 *Nanotechnology* **22** 265104
- [21] Navitski A, Lagotzky S, Reschke D, Singer X and Müller G 2013 *Physical Review Special Topics-Accelerators and Beams* **16** 112001
- [22] Nagaoka K, Fujii H, Matsuda K, Komaki M, Murata Y, Oshima C and Sakurai T 2001 *Applied surface science* **182** 12–19
- [23] Engelberg E Z, Ashkenazy Y and Assaf M 2018 *Physical Review Letters* **120** 124801
- [24] CLIC, CLICdp, Charles T, Giansiracusa P, Lucas T, Rassool R, Volpi M, Balazs C, Afanaciev K, Makarenko V, Patapenka A, Zhuk I et al. 2018 *CERN Yellow Reports* **2** (Preprint <https://arxiv.org/abs/1812.06018>) URL <https://e-publishing.cern.ch/index.php/CYRM/issue/view/66>
- [25] Timko H, Sjobak K, Methner L, Calatroni S, Djurabekova F, Matyash K, Nordlund K, Schneider R and Wuensch W 2014 From field emission to vacuum arc ignition: a new tool for simulating copper vacuum arcs submitted to Contributions to Plasma Physics
- [26] Wuensch W 2013 20 p URL <http://cds.cern.ch/record/1694664>
- [27] Tsong T and Kellogg G 1975 *Physical Review B* **12** 1343
- [28] Wang S and Tsong T 1982 *Physical Review B* **26** 6470
- [29] Häkkinen H, Merikoski J, Manninen M, Timonen J and Kaski K 1993 *Physical Review Letters* **70** 2451
- [30] Wang L and Clancy P 2001 *Surface Science* **473** 25–38
- [31] Lam C H, Lee C K and Sander L M 2002 *Physical Review Letters* **89** 216102
- [32] Zhang P, Zheng X, Wu S, Liu J and He D 2004 *Vacuum* **72** 405–410
- [33] Kara A, Trushin O, Yildirim H and Rahman T S 2009 *Journal of Physics: Condensed Matter* **21** 084213

- [34] Nandipati G, Kara A, Shah S I and Rahman T S 2012 *Journal of Computational Physics* **231** 3548–3560
- [35] Jansson V, Baibuz E and Djurabekova F 2016 *Nanotechnology* **27** 265708 (*Preprint* <https://arxiv.org/abs/1508.06870>) URL <http://arxiv.org/abs/1508.06870>
- [36] 2014 Kimocs — a Kinetic Monte Carlo simulation code for surfaces Available under the terms of the GNU General Public License. URL <https://gitlab.com/vjansson/Kimocs>
- [37] Vigonski S, Jansson V, Vlassov S, Polyakov B, Baibuz E, Oras S, Aabloo A, Djurabekova F and Zadin V 2018 *Nanotechnology* **29** 015704 (*Preprint* <http://arxiv.org/abs/1709.09104>) URL <http://arxiv.org/abs/1709.09104>
- [38] Zhao J, Baibuz E, Vernieres J, Grammatikopoulos P, Jansson V, Nagel M, Steinhauer S, Sowwan M, Kuronen A, Nordlund K *et al.* 2016 *ACS nano* URL <http://pubs.acs.org/doi/abs/10.1021/acsnano.6b01024>
- [39] Vurpillot F, Parviainen S, Djurabekova F, Zanuttini D and Gervais B 2018 *Materials Characterization* **146** 336–346
- [40] Djurabekova F, Parviainen S, Pohjonen A and Nordlund K 2011 *Physical Review E* **83** 026704
- [41] Parviainen S, Djurabekova F, Pohjonen A and Nordlund K 2011 *Nuclear Instruments and Methods in Physics Research Section B: Beam Interactions with Materials and Atoms* **269** 1748–1751
- [42] Veske M, Parviainen S, Zadin V, Aabloo A and Djurabekova F 2016 *Journal of Physics D: Applied Physics* **49** 215301 URL <https://arxiv.org/abs/1601.00407>
- [43] Wang P I, Zhao Y, Wang G and Lu T 2004 *Nanotechnology* **15** 218
- [44] Amram D, Kovalenko O, Klinger L and Rabkin E 2015 *Scripta Materialia* **109** 44–47
- [45] Soisson F and Fu C C 2007 *Physical Review B* **76** 214102
- [46] Vincent E, Becquart C, Pareige C, Pareige P and Domain C 2008 *Journal of Nuclear Materials* **373** 387–401
- [47] Castin N, Pascuet M I and Malerba L 2011 *The Journal of chemical physics* **135** 064502
- [48] Baibuz E, Vigonski S, Lahtinen J, Zhao J, Jansson V, Zadin V and Djurabekova F 2018 *Computational Materials Science* **146**(C) 287–302 URL <https://doi.org/10.1016/j.commatsci.2017.12.054>
- [49] Jansson V, Kyritsakis A, Vigonski S, Baibuz E, Zadin V, Aabloo A and Djurabekova F 2019 Submitted for publication (*Preprint* <https://arxiv.org/abs/1909.03519>) URL <https://arxiv.org/abs/1909.03519>
- [50] Olewicz T, Antczak G, Jurczyszyn L, Lyding J W and Ehrlich G 2014 *Phys. Rev. B* **89**(23) 235408
- [51] Jackson J 1975 *Classical electrodynamics* (Wiley, New York) ISBN 9780471431329
- [52] Press W H, Teukolsky S A, Vetterling W T and Flannery B P 1992 *Numerical recipes in C: Art of Scientific Computing, 2nd ed.* (Cambridge University Press, New York)
- [53] Fujita S and Shimoyama H 2007 *Physical Review B* **75** 235431
- [54] Stukowski A 2010 *Modelling and Simulation in Materials Science and Engineering* **18** 015012 URL <http://ovito.org/>